

Experimental Validation of the Docking Orientation of Cdc25 with Its Cdk2–CycA Protein Substrate[†]

Jungsan Sohn,^{‡,§} Jerry M. Parks,^{§,||} Gregory Buhman,[‡] Paul Brown,[‡] Kolbrun Kristjánssdóttir,[‡] Alexias Safi,[‡] Herbert Edelsbrunner,[⊥] Weitao Yang,^{||} and Johannes Rudolph^{*,‡}

Department of Computer Science, Duke University, Durham, North Carolina 27708, Department of Chemistry, Duke University, Durham, North Carolina 27708, and Department of Biochemistry, Duke University Medical Center, Durham, North Carolina 27710

Received August 24, 2005; Revised Manuscript Received October 21, 2005

ABSTRACT: Cdc25 phosphatases are key activators of the eukaryotic cell cycle and compelling anticancer targets because their overexpression has been associated with numerous cancers. However, drug discovery targeting these phosphatases has been hampered by the lack of structural information about how Cdc25s interact with their native protein substrates, the cyclin-dependent kinases. Herein, we predict a docked orientation for Cdc25B with its Cdk2-pTpY–CycA protein substrate by a rigid-body docking method and refine the docked models with full-scale molecular dynamics simulations and minimization. We validate the stable ensemble structure experimentally by a variety of in vitro and in vivo techniques. Specifically, we compare our model with a crystal structure of the substrate-trapping mutant of Cdc25B. We identify and validate in vivo a novel hot-spot residue on Cdc25B (Arg492) that plays a central role in protein substrate recognition. We identify a hot-spot residue on the substrate Cdk2 (Asp206) and confirm its interaction with hot-spot residues on Cdc25 using hot-spot swapping and double mutant cycles to derive interaction energies. Our experimentally validated model is consistent with previous studies of Cdk2 and its interaction partners and initiates the opportunity for drug discovery of inhibitors that target the remote binding sites of this protein–protein interaction.

Cdc25 phosphatases are important regulators of the eukaryotic cell cycle through their activation of the cyclin-dependent kinases (Cdk–Cyc)¹ (1). In humans, Cdc25A has a general role in controlling both the G1-to-S and G2-to-M transitions, whereas Cdc25B and Cdc25C regulate the G2-to-M transition by their activation of the Cdk1–CycB, Cdk1–CycA, and Cdk2–CycA complexes. In addition to their control of normal cell cycle progression, both the Cdc25A and Cdc25C homologues have been shown to integrate signals from checkpoint control in response to damage by ionizing radiation, ultraviolet light, and DNA-damaging agents (2). Because overexpression of Cdc25A and Cdc25B has been linked to numerous cancers and often correlates with a poor clinical outcome, efforts have been directed at developing specific inhibitors of Cdc25. However,

as for many other protein phosphatases, the Cdc25s have been recalcitrant to potent inhibition by small molecules. These failures arise from three obstacles presented by the active sites of the Cdc25 phosphatases. First, as seen in the crystal structure of the catalytic domains of Cdc25A and Cdc25B (3, 4), the active site region is shallow and does not provide a suitable pocket for binding of small molecule inhibitors. Second, although showing no homology to other protein phosphatases, the Cdc25s share the highly reactive active site cysteine of other protein tyrosine phosphatases, hampering screening and design efforts. Third, most studies of Cdc25 have used small molecule substrates, and thus, there is a lack of knowledge about the structural and mechanistic details of the reaction of Cdc25 with its native protein substrate, the bis-phosphorylated Cdk–cyclin complex (e.g., Cdk2-pTpY–CycA). The shallow active site and the low and nonspecific activity observed with peptidic substrates (5) emphasize that protein substrate recognition is an essential element of the catalytic reaction. In support of this concept, we have recently demonstrated the in vitro and in vivo relevance of two hot-spot mutations more than 25 Å from the active site of Cdc25B that are specifically important in the recognition of the bis-phosphorylated protein substrate (6). Although the individual structures of the Cdk2–CycA complex (PDB entry 1fin) and Cdc25B (PDB entry 1qb0) are known, no crystal structure of Cdc25B complexed to its protein substrate exists. Thus, the details of the essential interactions at the protein interface have not yet been elucidated.

[†] This work was funded by NIH Grant R01 GM61822 (J.R.), NIH Grant R01 GM061870 (W.Y.), and NSF Grant CCR-00-86013 (H.E.).

* To whom correspondence should be addressed. Telephone: (919) 668-6188. Fax: (919) 613-8642. E-mail: rudolph@biochem.duke.edu.

[‡] Department of Biochemistry, Duke University Medical Center.

[§] These authors contributed equally to this work.

^{||} Department of Chemistry, Duke University.

[⊥] Department of Computer Science, Duke University.

¹ Abbreviations: Cdk–Cyc, cyclin-dependent kinases; Cdk2-pTpY–CycA, threonine 14 and tyrosine 15 bis-phosphorylated Cdk2–CycA complex; MALDI, matrix-assisted laser desorption ionization; pNPP, *p*-nitrophenyl phosphate; mFP, 3-*O*-methylfluorescein phosphate; MD, molecular dynamics; rmsd, root-mean-square deviation; PTP1b, protein tyrosine phosphatase 1B; GVBD, germinal vesicle breakdown; CAK, Cdk-activating kinase; PME, particle mesh Ewald; CASP, critical assessment of structure prediction; CAPRI, critical assessment of predictions of interactions.

Given two individually crystallized proteins, one might presume that an orientation for protein docking could be readily obtained using computational methods. In fact, as evidenced by recent results from the CAPRI docking contest (7) (analogous to the CASP protein structure prediction contest), computational protein–protein docking is still an inexact science. Accurate scoring functions able to search the large space of all possible translations and rotations that also incorporate protein side chain and backbone flexibility do not exist. The dearth of predictive tools is particularly apparent when it is desirable to identify the molecular details of the protein–protein interaction, including potential hot-spot residues. The common practice of predicting multiple diverse docking orientations expands the list of possible mutations that need to be tested beyond practical limits. Accurate prediction of key interactions at a protein interface is difficult even for docking orientations that deviate by only 2–5 Å (by rmsd) from the “correct” answer, particularly since it is known that only a few of the contacting residues at a given protein interface contribute significantly to the binding specificity (8).

In the case of the protein–protein interactions that govern substrate recognition for the Cdc25 phosphatase, specific knowledge of points of contact potentially simplifies the predictive protein docking problem. First, the active site cysteine of Cdc25, known to form a phosphocysteine intermediate, must come close to the preferred site of dephosphorylation (Thr14) on the bis-phosphorylated Cdk2-pTpY–CycA complex. On Cdc25B, the crystal structure containing a bound sulfate at the active site is expected to be a good representation of the phosphate group of the phosphorylated protein substrate. However, on the Cdk2-pTpY–CycA substrate, the exact orientation of the β -hairpin loop encompassing the adjacent Thr14 and Tyr15 sites of phosphorylation is unknown. The crystal structure of the unphosphorylated complex makes it evident that the β -hairpin loop must extend outward at least somewhat to accommodate a bulky phosphate on the partially buried Tyr15 (9). The second point of contact between Cdc25B and its protein substrate is known only for the Cdc25 side of the interaction and encompasses the recently identified hot-spot residues (Arg488 and Tyr497) that are >20 Å from the active site. These two hot-spot residues are expected to make contact with either Cdk2 or cyclin A at a binding interface. On the basis of the evolutionary conservation of these hot-spot residues in the Cdc25s, this contact is presumably through completely conserved residues on the protein substrate. Such potential residues are not easily selected however, given the high degree of overall conservation of residues in the Cdk/cyclin family, particularly for the Cdks. Also, a large (>50) number of residues 20 ± 10 Å from the site of dephosphorylation exist. Thus, although additional biochemical information simplifies the problem for predicting the docking orientation between the Cdk2-pTpY–CycA substrate and Cdc25 phosphatase, this is still a difficult problem.

Herein, we propose by computational docking, refine by molecular dynamics, and validate by X-ray crystallography, site-directed mutagenesis, hot-spot swapping, and double mutant cycle analysis a docked orientation for the Cdc25–Cdk2-pTpY–CycA complex. Our docked orientation is useful for further investigating the molecular details of transient protein substrate recognition by the Cdc25 phos-

phatase and the development of specific protein–protein interaction inhibitors with therapeutic potential as anticancer agents.

MATERIALS AND METHODS

Coarse Docking and Local Improvement. Coarse docking was implemented as described previously (10). Briefly, feature points consisting of protrusions or cavities and their corresponding saddles are found for the surfaces generated from the PDB entries for Cdc25B (1qb0) and the Cdk2–CycA complex (1fin) (11). After filtering based on length (3.0 Å) or elevation (0.2 Å) was carried out, the alignment procedure matches significant features of 1fin with significant features of 1qb0. The alignments are ranked by counting the number of nonoverlapping spheres at a distance of at most 1.5 Å, allowing up to 60 overlapping atom pairs to account for side chain flexibility during docking. The top 2000 scoring solutions are next further refined using a local improvement algorithm (12). Briefly, weighted least-squares minimization is used to improve favorable atomic contacts in an outer loop and reduce unfavorable overlaps in an inner loop. The resulting 2000 locally improved solutions were then filtered for a tether distance of less than 10 Å from Cys473 *Sy* in Cdc25B to Thr14 *Oy* in Cdk2.

Refinement by Molecular Dynamics. Two rigid-body docking solutions (models 1 and 2) were subjected to further refinement by molecular dynamics. Cys473 in Cdc25B was converted to Ser by changing the sulfur atom to oxygen (see Results), and bis-anionic phosphates were added manually to Thr14 and Tyr15 of Cdk2. Hydrogen atoms were added to the complex using MolProbity (13), and the docked complexes were subjected to 5000 steps of conjugate gradient minimization in the gas phase without restraints. Each system was then solvated in a box of TIP3P waters (14) with a minimum distance of 14 Å from the protein to the face of the box. The complete system consisted of 116 180 atoms, including 12 002 protein atoms and 34 726 water molecules. The overall charge of the system was -3 , and no counterions were added. Following solvation, a restraint potential of $99 \text{ kcal mol}^{-1} \text{ \AA}^{-1}$ was placed on all α -carbons, and the system was minimized for 3000 steps, followed by molecular dynamics for 300–500 ps at 150 K. Periodic boundary conditions were used, and the system was treated with PME electrostatics (15) with grid dimensions of 100, 100, and 125 Å. The RATTLE algorithm (16) was used to constrain all bonds to hydrogen to their equilibrium distances, and multiple time steps of 6, 2, and 2 fs were used for long-range electrostatic, short-range nonbonded, and short-range bonded terms, respectively. A 12.0 Å nonbonded cutoff was used in all dynamics simulations. The Charmm27 force field (17) was used for the simulation with additional parameters for phosphotyrosine (18). All molecular dynamics simulations were carried out using NAMD2 (19). Following molecular dynamics at 150 K, up to 1 ns of molecular dynamics was performed without restraints. The temperature was increased gradually from 150 to 300, 305, 310, or 400 K, and the pressure was adjusted to 1 atm. These values were then maintained for the duration of the simulation. Individual snapshots in the simulation were subjected to 10 000 steps of minimization.

X-ray Crystallography. Cdc25B(C473S) was purified (20) and crystallized (21) as previously described for the wild-

type protein. Cdc25B crystallizes with the symmetry of space group $P2_12_12_1$ with one molecule in the asymmetric unit. Prior to data collection, the crystallization mother liquor was replaced with a buffer solution containing 100 mM Tris-HCl (pH 7.25), 100 mM NaCl, 25% polyethylene glycol 3350, and 10% glycerol by extensive buffer exchange to provide cryoprotection for data collection following flash-freezing in liquid nitrogen. Data were collected at a wavelength of 1 Å at 100 K at the SER-CAT synchrotron beamline, Advanced Photon Source (Argonne, IL). Crystallography and NMR System (CNS) (22) was used for all reciprocal space refinement, with a randomly selected 10% of the unique reflections reserved for calculation of R_{free} (23). O (24) was used for manual rebuilding of the model with visualization of $F_o - F_c$ and $2F_o - F_c$ electron density maps, contoured at 3σ and 1σ , respectively. The initial round of refinement consisted of rigid-body minimization followed by energy minimization and B-factor refinement with CNS starting from a protein-only model of apo-Cdc25B [PDB entry 1YMK (21)]. Data collection and refinement statistics are given in Table 1 of the Supporting Information, and the coordinates have been deposited in the Protein Data Bank (entry 2A2K).

Mutagenesis and Protein Expression and Purification. Each mutant construct of human Cdc25B and human Cdk2 was prepared using the QuikChange protocol from Stratagene and the appropriate primer pair. The wild type and each mutant of the catalytic domain of Cdc25B were purified to homogeneity as untagged proteins following expression in *Escherichia coli* as described previously (20). Full-length wild-type and mutant Cdk2s were expressed as six-His-tagged proteins from Sf9 cells using the baculovirus expression system (Invitrogen). The Cdk2 protein was purified by NTA affinity chromatography as described by the manufacturer (Qiagen) and was dialyzed against 40 mM HEPES (pH 7.0), 50 mM NaCl, and 2 mM DTT prior to formation of the complex with cyclin A. The bis-phosphorylated Cdk2-pTpY-CycA complex, in which cyclin A encompasses residues 174–432 and with quantitative phosphorylation by kinase Myt1 on Thr14 and Tyr15 of Cdk2, was prepared as previously described (5). Cdk2-pTY was prepared by treating Cdk2-pTpY with 0.5 equiv of PTP1b (a generous gift from Z.-Y. Zhang, Albert Einstein College of Medicine, Bronx, NY) for 1 h followed by the subsequent removal of the released inorganic phosphate by G-50 gel filtration. All mutations were confirmed by DNA sequencing and matrix-assisted laser desorption ionization (MALDI) mass spectrometry with post-source decay sequencing of tryptic fragments.

Kinetic Assays. All phosphatase reactions were performed at 25 °C in a three-component buffer [50 mM Tris, 50 mM Bis-Tris, and 100 mM sodium acetate (pH 6.5)] containing 2–5 mM DTT. Reactions using *p*-nitrophenyl phosphate (pNPP) and 3-*O*-methylfluorescein phosphate (mFP) were followed by continuous UV-vis spectroscopy at 410 nm ($\epsilon = 5142 \text{ M}^{-1} \text{ cm}^{-1}$) and 477 nm ($\epsilon = 27\,200 \text{ M}^{-1} \text{ cm}^{-1}$), respectively. All assays using pNPP and mFP consisted of complete K_m determinations using eight concentrations of substrate between $0.2K_m$ and $5K_m$, and the data were fitted to Cleland's equations (25). The bis-phosphorylated Cdk2-pTpY-CycA complex (200–500 Ci/mol) was assayed by monitoring the release of inorganic phosphate following

precipitation of unreacted substrate by trichloroacetic acid as described previously (5). Assays using the Cdk2-pTpY-CycA substrate (30–150 nM) were strictly limited to k_{cat}/K_m determinations wherein time dependence (five points minimum), substrate concentration dependence (two to three differing concentrations), and enzyme concentration dependence (five to six differing concentrations) were employed for each assay. Differences in k_{cat}/K_m values between mutants for the double mutant cycles were converted to free energy using the relation $\Delta\Delta G = -RT \ln[(k_{\text{cat}}/K_m)_{\text{mut}}/(k_{\text{cat}}/K_m)_{\text{WT}}]$, where R is the gas constant and T is the temperature in kelvin. Error propagation analysis for the double mutant cycles was performed as described previously (26). Kinase reactions using Cdk2-CycA as an enzyme with histone as a substrate were performed by monitoring incorporation of ^{32}P from [γ - ^{32}P]ATP in a filter-based assay following precipitation with trichloroacetic acid, as described previously (5, 9).

Cell-Based Assays. Cdc25B (1 μM final concentration) was injected into stage VI oocytes from *Xenopus laevis*. Cdc25-induced germinal vesicle breakdown (GVBD) and the kinase activity of the immunoprecipitated Cdk2-cyclin B complex with histone substrate were monitored as previously described (6). The presence of Cdc25B protein in the oocytes was confirmed by Western blot analysis using an antibody to the C-terminus (Santa Cruz Biotechnology, Santa Cruz, CA). In *Saccharomyces cerevisiae*, *mih1* is the only *cdc25* homologue and deletion of the *wee1* regulator *hsl7* yields a *mih1*-dependent phenotype (27). The JMY1290 (*hsl7* Δ Gal-MIH1 *leu2*) yeast strain was transformed with an integrating plasmid containing *myc*-tagged WT, C473S, or R492L equivalents of *mih1(cdc25)* under the control of its genomic promoter. The phenotype of multiple transformants containing the newly introduced *mih1* was visualized by microscopy as previously described (6), and the expression of MIH1 in these transformants was confirmed by Western blotting using the Myc antibody.

RESULTS

Coarse Docking with Local Improvement. We began our efforts to identify a docking orientation for Cdc25 and the Cdk-CycA complex by applying a two-step rigid-body docking method. We justified initially treating Cdc25 and the Cdk2-CycA complex as rigid bodies as we were not expecting any major conformational changes to occur upon protein association. The catalytic domain of Cdc25 is a compact protein in which major structural changes would appear to yield only unfolded protein. Its interaction partner Cdk2-CycA has been crystallized more than 90 times in complex with numerous other proteins and small molecules. Although some side chains or loops are subject to significant movements, the core fold of the protein remains highly static. In fact, the backbone rmsd of the kinase domain of Cdk2 compared to the divergent cAMP-dependent protein kinase is only 1.4 Å. The first step in our docking method is based on aligning feature points identified by the elevation function, a tool that extracts major knobs and holes along with their relative size and orientation (11). Despite treating proteins as rigid bodies, this first coarse step is useful for the prediction of a limited number of possible orientations for solving the "unbound" protein-protein docking problem (10). [Unbound docking uses the structures of individually crystallized proteins to predict suitable docking orientations,

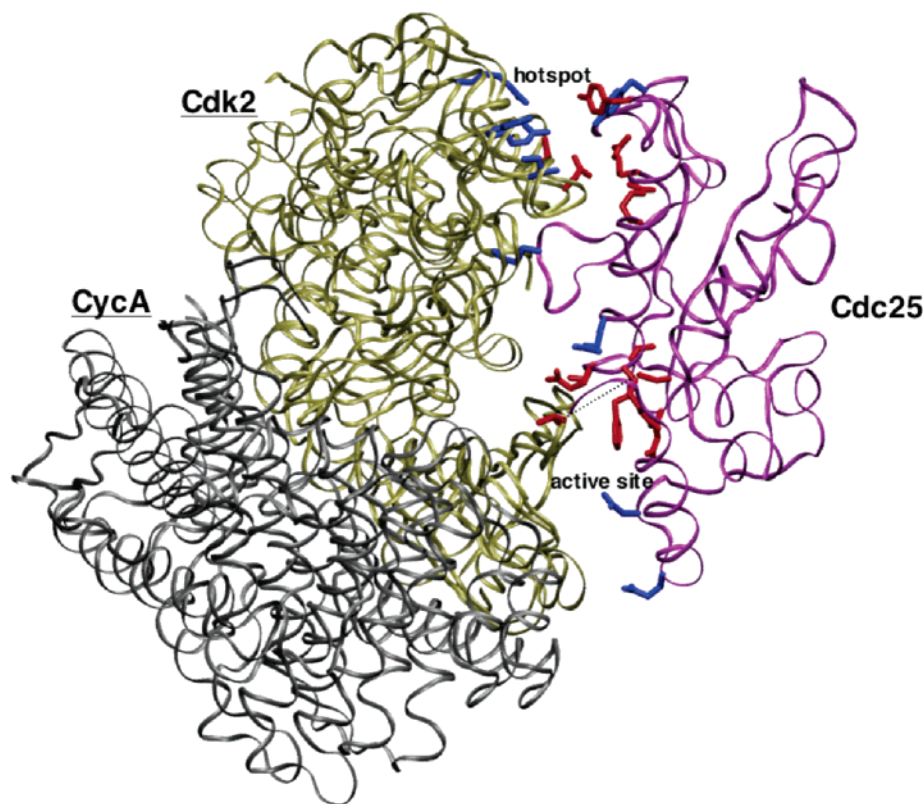


FIGURE 1: Overlay of locally improved model 1 and model 2 from rigid-body docking, wherein Cdc25B is fixed. Cdk2 is colored tan, CycA gray, and Cdc25 purple. The residues comprising the active site of Cdc25 and Thr14 of Cdk2 as well as the remote hot-spot site (Arg488, Arg492, and Tyr497 of Cdc25 and Asp206 of Cdk2) are shown as licorice bonds in red. Other residues whose mutation does not affect activity despite being located at the protein interface are shown as licorice bonds in blue. The tether distance between Cys473 S γ and Thr14 O γ is represented as a black dotted line.

and methods can be tested using a benchmark database (28).] The second step in our docking method is based on weighted least-squares motions that maximize the pairs of contacting residues while minimizing the number of atom overlaps (12). Applying the coarse alignment method to docking of Cdc25B to the Cdk2–CycA complex, we generated the top 2000 scoring orientations, expecting to obtain at least one or more solutions representative of the true docking orientation (within 7 Å of the overall rmsd). Applying a tether filter in which the active site Cys473 S γ is expected to be less than 10 Å from the unphosphorylated Thr14 O γ of the product, we found seven different orientations ranked from 92 to 1422 in the top 2000 scoring solutions. The diversity of these orientations is exemplified by the large pairwise rmsds of Cdk2 compared to a fixed Cdc25B, ranging from 1.7 to 62 Å. Following application of the local improvement algorithm to increase the geometric complementarity and reduce the number of overlaps, the solutions initially ranked 92 (model 1) and 448 (model 2) showed the Arg488 or Tyr497 hot-spot residues on Cdc25B at the protein interface while maintaining a 8.4 Å Cys473 S γ –Thr14 O γ tether distance (Figure 1). Intriguingly, the carboxylate oxygens of Asp206 on Cdk2 are only 5–7 Å from the δ -guanidino groups of the previously described hot-spot residue Arg488 (6) and another arginine, Arg492, suggesting possible formation of salt bridges at the protein interface. Thus, the similar orientations of models 1 and 2 predicted by the rigid-body docking are consistent with the biochemical data and served as a starting point for further refinement and experimental testing.

Refinement by Molecular Dynamics. The limitations of rigid-body docking for identifying key contact residues are numerous. Even a slightly incorrect docked orientation that has not accounted for side chain rearrangements expected to occur during complex formation will yield false residue pairings at the interface. Molecular dynamics can provide a useful and powerful refinement that may lead to the accurate identification of new hot-spot residues and thus allow a successful interplay between theory and experiment. Therefore, further refinement of the proposed docking orientations was undertaken using full-scale molecular dynamics of the entire complex. To more accurately reflect the enzyme-bound substrate complex and to compare our results with experimental data, two modifications of the models generated by the rigid-body docking were performed. First, as the preferred substrate is the bis-phosphorylated Cdk2-pTpY–CycA complex, we added phosphates to both Thr14 and Tyr15 of Cdk2. Second, because it is known that the active site C473S mutant has no activity and instead binds tightly to the protein substrate (known as a substrate-trapping mutant) (6, 29), we incorporated this mutation into our simulations to favor formation of a bound protein complex. The two rigid-body docked solutions (models 1 and 2) were then used for refinement by molecular dynamics and minimization. Molecular dynamics (MD) at 300 K for model 2 yielded a stable overall rmsd ($\Delta < 2.1$ Å) relative to the gas-phase minimized starting configuration after ~ 200 ps. Also, distances between key interfacial residues (hydrogen bond donor–acceptor distances) were stabilized with standard deviations of 0.2–0.4 Å over 800 ps (see below). In contrast, for model

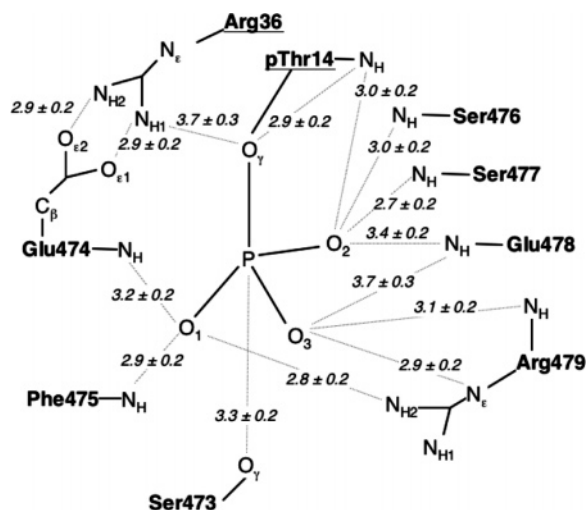


FIGURE 2: Active site of Cdc25B(C473S) that cradles pThr14 of the Cdk2-pTpY-CycA complex. Average distances (heavy atom-heavy atom) observed for the MD trajectory at 305 K taken from 200 to 1000 ps (160 snapshots). Residues from Cdk2 are underlined. Similar results were observed for independent MD simulations at 300 and 310 K.

1, while the overall rmsd also was stabilized ($\Delta < 2.1$ Å), the interfacial residues in the hot-spot region had significantly larger distance fluctuations as demonstrated by standard deviations of 0.4–0.8 Å. To further probe the refinement of model 2 by MD, we ran trajectories for 800–1000 ps at varying temperatures and saw essentially identical results at 305 and 310 K, with a slight steady increase in the rmsd (0.75 Å) but preservation of interfacial contacts at 400 K. To describe and evaluate interfacial contacts between Cdc25B and the Cdk2-pTpY-CycA substrate, we chose the ensemble structure of the last 800 ps of MD stabilization from the simulation at 305K (Supporting Information file available). We discuss next some key findings from this ensemble structure and validate our observations experimentally using X-ray crystallography, site-directed mutagenesis, hot-spot swapping, and double mutant cycles.

The Active Site Loop of Cdc25 Cradles pThr14. The active site of Cdc25B in the refined complex represents well the substrate-trapping nature of the C473S mutant. The pThr14, the first phosphate to be removed from the Cdk2-pTpY-CycA substrate (5, 30), has moved more than 3.5 Å into the phosphate-binding cradle of the active site (Figure 2). As expected from numerous crystal structures of other protein tyrosine phosphatases usually complexed with sulfate or phosphate, the phosphate of pThr14 makes numerous hydrogen bonds to the backbone amides of the active site loop as well as to the side chain of Arg479 of the conserved CX₅R active site motif. The phosphate is additionally coordinated in the active site pocket by contributions from the protein substrate, namely, the amide backbone of Thr14 and the side chain of Arg36 (Figure 2). The hydroxyl group of the “mutated” Ser473 is positioned beneath the phosphate, in a good location to mimic nucleophilic attack of the active site cysteine. The active site pocket is tightly packed with residues coming from Cdc25 and Cdk2 and no apparent space for any water molecules. Interestingly, attempts to use molecular dynamics to refine the structures of the docked complex that had not undergone the local improvement procedure led to little or no observable binding of phospho-

threonine in the active site loop, emphasizing the importance of this second step in the rigid-body docking protocol. Thus, it appears that binding of the protein substrate to Cdc25 phosphatase creates a solvent-excluded environment conducive to formation of the meta-phosphate-like transition state, explaining in part the 6 order of magnitude greater rate of reactivity of protein substrate compared to those of peptidic substrates containing the same primary sequence (5).

To compare the details of our model at the active site with experimental data, we determined the crystal structure of the C473S mutant of Cdc25B. The structure of C473S, refined to 1.5 Å (R and $R_{\text{free}} = 18.2$ and 19.1%, respectively), shows an essentially identical structure compared to wild-type Cdc25B with a rmsd for the C α atoms of 0.23 Å. The active site loops are also superimposable with a rmsd for the C α atoms of residues 472–479 of 0.13 Å. This high degree of similarity between wild-type Cdc25B and its substrate-trapping mutant does not hold true for all protein tyrosine phosphatases. For example, the C215S mutant of protein tyrosine phosphatase 1B (PTP1b) (31) shows a significantly distorted active site loop that is expected to undergo rearrangement to accommodate tight binding of protein substrate. The active site loop in the C473S structure of Cdc25B contains a tightly bound sulfate in the active site that mimics phosphate binding. A second bound sulfate is seen coordinated between Arg488 and Arg492. Previous experiments with wild-type Cdc25B have shown that buffer exchange removes both bound sulfates from Cdc25B, which allowed characterization of the apoprotein (21). As an indication of how tightly sulfate is bound in the C473S mutant, only the remote sulfate could be removed following extensive buffer exchange.

The overlay of the experimental structure of C473S with the refined complex determined by molecular dynamics shows excellent agreement (rmsd = 1.5 Å for C α atoms). The active site residues from His472 to Arg479 can be superimposed with a C α rmsd of only 0.6 Å (Figure 3). The only significant differences at the active site between the two structures arise as a result of subtle differences induced by the protein substrate that help account for its tight binding to the mutated enzyme. For example, in the model Phe475 twists by approximately 45° compared to the crystal structure to accommodate and interact with the side chain of Arg36 from Cdk2 (Figure 3). Additionally, Ser477 in the model adopts an alternative conformation to avoid steric clashes with pThr14 (not shown). Finally, Arg479 moves 0.9 Å closer to the phosphate in the model than is seen for the sulfate in the crystal structure to make more favorable H-bond interactions with O₁ and O₃ (Figures 2 and 3), perhaps because of subtle differences in size and charge in phosphate versus sulfate.

pTyr15 Is Not Involved in Binding of the Cdk2-pTpY-CycA Complex. Cdc25 is a dual-specificity phosphatase whose preferred protein substrate is bis-phosphorylated and whose mechanism proceeds via sequential dephosphorylation of pThr14 prior to pTyr15 (5, 30). In our model, pTyr15 has rotated outward (the oxygen has moved >9 Å) to accommodate the bulk of the phosphate, with little distortion of the backbone atoms in the β -hairpin loop (Figure 4). The phosphate of pTyr15 interacts almost exclusively with Cdk2, coordinated by Arg50, Arg150, and Ser46, suggesting that pTyr15 does not contribute significantly to binding of the

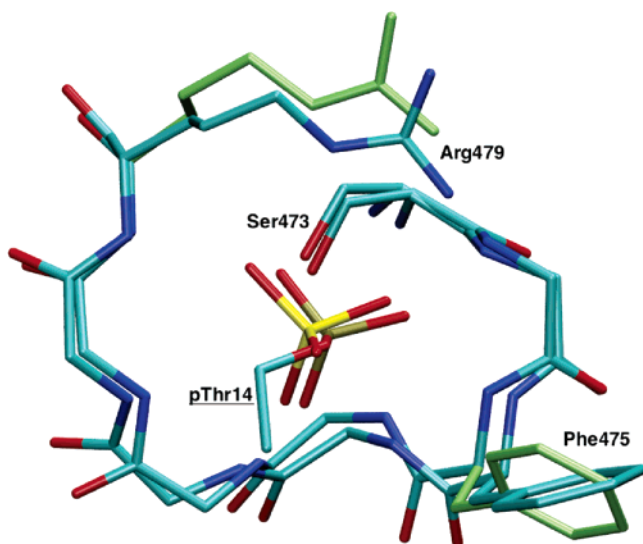


FIGURE 3: Overlay of the active site loop of the docked orientation refined by MD and the C473S mutant determined by X-ray crystallography. For clarity, backbone atoms are shown for only residues 474 and 476–478 using CPK coloring. Side chains of Phe475 and Arg479 in the crystal structure are colored light green. The sulfate from the crystal structure has a yellow sulfur, and the phosphate from pThr14 (truncated at C α) in the model has a tan phosphorus.

bis-phosphorylated substrate by Cdc25. The closest atom from Cdc25B to pTyr15 is Trp550, making a long hydrogen bond with O γ of pTyr15. We tested the validity of this region of our model by measuring the activity for two pTyr15-dephosphorylated variants of the protein substrate, expecting no dramatic differences in activity. First, we prepared the Cdk2-pTY–CycA substrate by treatment of the Cdk2-pTpY–CycA substrate with PTP1b. This tyrosine phosphatase exclusively removes the phosphate from pTyr15, as confirmed by phospho-amino acid analysis (data not shown). The activity for the Cdk2-pTY–CycA complex was reduced by a factor of only 2, indicating that pTyr15 does not contribute significantly to substrate recognition (Table 1). Second, we prepared the Cdk2-pTF–CycA complex in which the Cdk2 subunit contains a Y15F mutation. The change in activity for this modification was also only modest (Table 1). Thus, in accord with our model, pTyr15 is not an important element of substrate recognition for Cdc25B, at least for dephosphorylation of pThr14.

Identification of Arg492 as a Hot-Spot Residue on Cdc25B.

We have previously shown that Arg488 and Tyr497 of Cdc25B, located 20–30 Å from the active site loop, serve as crucial residues for the recognition of protein substrate both in vitro and in vivo (6). In the refined structure of the complex, Arg488 and Tyr497 contact Asp206 and Asp210 of Cdk2 (Figure 5), respectively, in agreement with the experimental data. However, Arg492 and not Arg488 or Tyr497 appears to be the most central residue of this remote hot spot by making a close ionic interaction with Asp206 of Cdk2. The distance between Arg492 and Asp210 is slightly greater, although we observe isolated snapshots in the molecular dynamics trajectory with a bridging water molecule between O $_{D1}$ of Asp210 in Cdk2 and N $_{HI}$ of Arg492 in Cdc25B (Figure 5). We tested the prediction that Arg492 could be an additional hot-spot residue experimentally by assaying the R492L mutant with the Cdk2-pTpY–CycA

protein substrate. The R492L mutant displayed only 0.5% activity compared to wild-type Cdc25B ($k_{cat}/K_m = 4200 \pm 500$ and $860\,000 \pm 80\,000\text{ M}^{-1}\text{ s}^{-1}$, respectively). The reduction in activity for the R492L mutant is comparable to those of the previously identified Arg488 (0.2%) and Tyr497 (0.4%) hot-spot residues (6). Confirming the integrity of the active site and the role of Arg492 specifically in protein recognitions in this mutant, we found R492L had unchanged activity with two small molecule substrates. The activities with *p*-nitrophenyl phosphate, a probe of the first half-reaction (formation of the phosphocysteine intermediate), and *O*-methylfluorescein phosphate, a probe of the second half-reaction (hydrolysis of the phosphocysteine intermediate), were essentially identical to those of wild-type Cdc25 for both k_{cat} and k_{cat}/K_m (data not shown). Phospho-amino acid analysis demonstrated that there was no change in mechanism compared to that of the wild-type protein, with sequential removal of phosphothreonine before phosphotyrosine (data not shown).

Like the two previously identified hot-spot residues, Arg488 and Tyr497, Arg492 is one of the few residues conserved in all known Cdc25s. This allowed us to probe the physiological significance of Arg492 in binding and correctly orienting the protein substrate for catalysis in two biological systems, *X. laevis* and budding yeast. In the *X. laevis* model for studying cell cycle, immature oocytes can be converted to fertilizable eggs by treatment with hormones such as progesterone. This oocyte maturation process ultimately results in the dephosphorylation and activation of the Cdc2–cyclin B complex and can be triggered more directly by microinjection of the Cdc25 protein (32, 33). Injection of wild-type Cdc25B, but not the active site mutant C473S or the hot-spot mutant R492L, leads to oocyte maturation, as visualized by monitoring formation of a white spot on the vegetal pole of the oocyte, indicative of germinal vesicle breakdown (GVBD) (Figure 6A). As expected, GVBD is accompanied by activation of Cdc2–cyclin B kinase activity, measured using histone substrates with the immunoprecipitated cyclin B complexes.

In the budding yeast *S. cerevisiae*, Mih1p, the single homologue of Cdc25, is essential for proper cell division in the absence of one of two (Hsl1p and Hsl7p) negative regulators of Swe1p, the kinase responsible for adding the inhibitory phosphates to the Cdc2–cyclin B targets of Mih1p (Cdc25). Using a yeast strain with an *hsl7* deletion and expressing Mih1p under control of the repressible *gal* promoter, we can introduce full-length wild-type *mih1* under control of its native promoter and recover normal cell growth on glucose (Figure 6B). In contrast, introduction of the corresponding active site C473S mutation or hot-spot R492L mutation leads to elongated hyphal cells incapable of proper cell division (Figure 6B). Thus, like the Arg488 and Tyr497 hot-spot residues, Arg492 is essential for cell viability in the context of the full-length protein under physiological conditions.

Identification of Asp206 as a Hot-Spot Residue on Cdk2.

To further test the predictions from the refined structure of the complex between Cdc25B and the Cdk2–CycA substrate, we prepared six site-specific mutants of Cdk2 in the region of the contact residues with Cdc25B, namely, D206A, I209A, D210A, F213A, R214A, and R217A. As expected from its central location in the remote hot-spot, D206A displayed

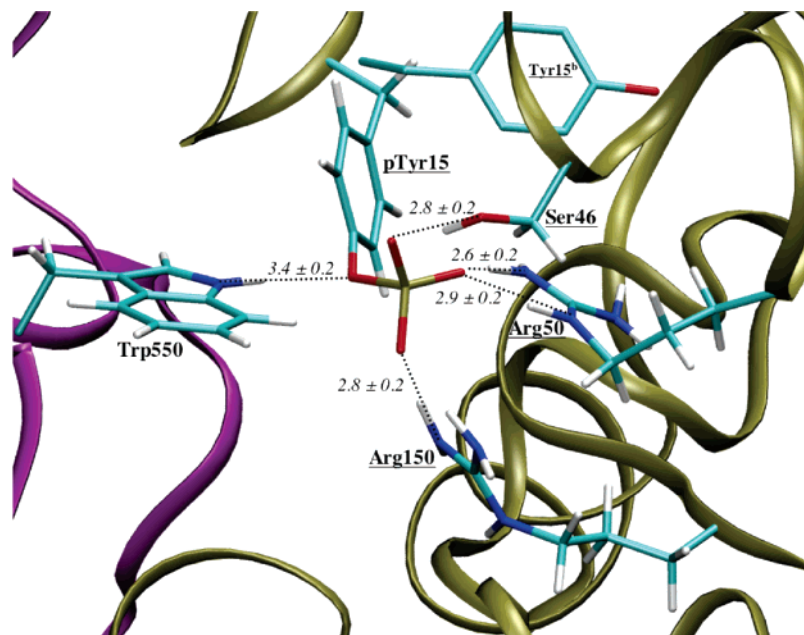


FIGURE 4: Phosphate binding site for pTyr15 located mostly on Cdk2. The backbone of Cdc25B is colored purple, and the backbone of Cdk2 is colored tan, with residues from Cdk2 underlined. The original location of Tyr15 in the unphosphorylated complex is also shown (Tyr15^b). Average distances were determined as described in the legend of Figure 2.

Table 1: Activity of Cdc25B with Various Forms of Protein Substrate

Cdk2-pTpY-CycA form	k_{cat}/K_m ($M^{-1} s^{-1}$)
WT	860000 ± 80000
pTY	406000 ± 45000
pTF	250000 ± 60000
D206A	1500 ± 300
I209A	110000 ± 45000
D210A	28000 ± 3000
F213A	580000 ± 80000
R214A	590000 ± 50000
R217A	720000 ± 57000

only 0.17% activity as a protein substrate for Cdc25 compared to the wild-type Cdk2-pTpY-CycA complex (Table 1). Mutations of Ile209 and Asp210 had smaller effects, with 13 and 3.2% residual activity, respectively, whereas the other three mutations caused no significant changes in activity (Table 1). Assigning the reduction in activity for these Cdk2 mutations specifically to the interaction with Cdc25 is bolstered by three tests of the integrity of the mutated proteins. First, Cdk2 complex formation with cyclin A was unaffected. Second, Cdk2-CycA kinase activity toward histone substrates, with or without activation by phosphorylation with Cdk-activating kinase (CAK), was essentially unchanged (data not shown). Finally, the quantitative phosphorylation of the Cdk2-CycA complex by Myt1 kinase to prepare the Cdk-pTpY-CycA substrate was unperturbed. Finding Asp206 as a hot-spot residue and Asp210 as a more weakly contributing residue is consistent with our docking model wherein these residues form hydrogen bonding interactions with the hot-spot residues of Cdc25B. These results are also consistent with prior work for other protein interactions wherein energetically critical residues on one protein tend to lie across from energetically critical residues on the other protein (34–36).

Swapping Hot-Spot Residues and Double Mutant Cycles. While the mutational data of Arg492 of Cdc25B and Asp206 of Cdk2 support our proposed docking orientation, several

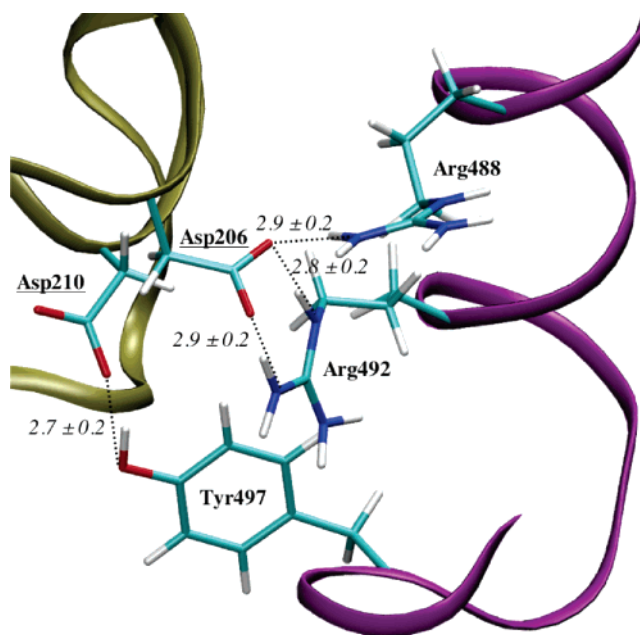


FIGURE 5: Remote hot-spot residues in Cdc25B (Arg488, Arg492, and Tyr497) interact with Asp206 and Asp210 of Cdk2. The backbone of Cdc25B is colored purple, and the backbone of Cdk2 is colored tan, with residues from Cdk2 underlined. Average distances were determined as described in the legend of Figure 2.

other explanations are possible. First, differences in activity for mutations of single residues alone reflect differences in free energy for the unbound and substrate-bound complexes. Thus, perturbed activities for such mutations may not solely reflect the intrinsic effects that can be attributed to such a residue's contribution to the interaction of interest. Second, it is possible that hot-spot residues Arg488, Arg492, and Tyr497 on Cdc25 make no contact with hot-spot residue Asp206 on Cdk2, instead forming as-yet-unidentified interactions in an alternative docking orientation not found by our computational procedures. These concerns can be ad-

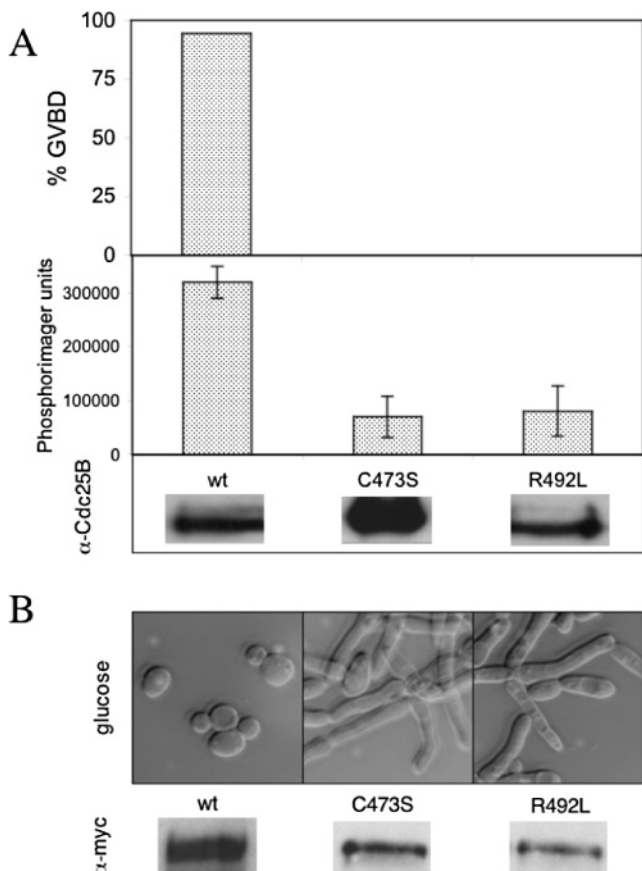


FIGURE 6: Arg92 is essential for Cdc25B function in vivo. (A) Cdc25 ($1 \mu\text{M}$ final concentration) was injected in stage VI oocytes (14–18 replicates per enzyme form), and GVBD was monitored by visual inspection. Histone kinase activity was tested from one to two pooled oocytes, and the presence of Cdc25B was demonstrated by Western blotting from six pooled oocytes using an antibody directed at the C-terminus of Cdc25B. (B) The JMY1290 (*hsl1 Δ GAL-MIH1 leu2*) yeast strain was transformed with a vector containing myc-tagged *mih1* WT, C473S, or R492L and subsequently grown in media containing glucose that represses the wild-type copy of *MIH1*. Note the elongated, hyphal growth in the strains that do not express functional Mih1 (Cdc25). Western blots using an antibody directed at the C-terminal Myc tag demonstrated expression of Mih1 in the transformed strains.

dressed by swapping hot-spot residues and by double mutant cycle experiments.

We began our attempt to swap two hot-spot residues by measuring the activity of the D206R mutant of Cdk2 and the R492D mutant of Cdc25. As expected, replacing the original charged residues with oppositely charged residues was at least as deleterious as the original more conservative hot-spot mutations. D206R in the Cdk2-pTpY-CycA complex assayed with wild-type Cdc25 showed only 0.09% activity ($k_{\text{cat}}/K_m = 800 \pm 150 \text{ M}^{-1} \text{ s}^{-1}$) compared to that of the wild-type substrate, whereas the R492D mutant of Cdc25 assayed with the wild-type Cdk2-pTpY-CycA complex exhibited only 0.5% activity ($k_{\text{cat}}/K_m = 4000 \pm 500 \text{ M}^{-1} \text{ s}^{-1}$) compared to that of the wild-type enzyme. Intuitively, if these two residues function independently, one would expect their activity with each other to be at least as low as the lower of the two (see double mutant cycles below). In contrast, if these two swapped residues re-establish a functional interaction, then one would expect to observe an increased activity compared to that of either of the single mutations. Indeed, we observe a dramatic recovery of activity

Table 2: Double Mutant Cycles

Cdc25B-Cdk2-pTpY-CycA	D206A	D210A
R488L	2.8 ± 0.4	1.3 ± 0.3
R492L	3.8 ± 0.4	1.9 ± 0.3
Y497A	1.6 ± 0.5	1.3 ± 0.4
without the C-tail	-0.03 ± 0.4	0.2 ± 0.3

in assaying the R492D mutant of Cdc25 with the D206R mutant of the Cdk2-pTpY-CycA complex, namely back to 27% of the original wild-type pair ($k_{\text{cat}}/K_m = 230\,000 \pm 20\,000 \text{ M}^{-1} \text{ s}^{-1}$).

We can further probe the interactions across the protein interface more quantitatively using double mutant cycles. Since their first introduction (37), double mutant cycles have proven to be a powerful tool for deciphering the energetic relationships between two or more residues on the same protein or across the interface of two interacting proteins (38–40). For two interacting proteins, a double mutant cycle involves comparing the activity of both wild-type proteins with the activity of a single damaging mutant of each and with the activity of the two mutants with each other. If the change in activity in this thermodynamic cycle, in terms of free energy, differs from simple additivity, then there exists an interaction or coupling energy ($\Delta\Delta G_{\text{int}}$) between the two residues (assuming no change in mechanism). Mathematically, this coupling energy is

$$\Delta\Delta G_{\text{int}} = \Delta\Delta G_1 + \Delta\Delta G_2 - \Delta\Delta G_{12}$$

where the $\Delta\Delta G$ values reflect the free energy changes for the two mutants together or separately as noted by the subscripts. Although the coupling energy is a purely thermodynamic term and cannot be used to derive direct molecular interactions, numerous previous studies demonstrate that mutations of two remote residues exhibit pure additivity with no coupling energy whereas residues within 5 \AA can exhibit significant coupling energies ($>2 \text{ kcal/mol}$) (41–43).

The double mutant cycles between the three hot-spot mutants on Cdc25B (R488L, R492L, and Y497A) and the hot-spot mutant on Cdk2 (D206A) validate our refined docking orientation (Table 2). Significant interaction energies were observed between all three hot-spots of Cdc25B and Asp206 of Cdk2. The largest pairwise coupling energy of 3.9 kcal/mol was found between Arg492 and Asp206, consistent with their proximity at the interface (Figure 5). Arg488 also exhibited a strong interaction energy with Asp206 (2.8 kcal/mol). Although as an individual mutation Asp210 of Cdk2 does not contribute nearly as much toward recognition by Cdc25B, in the context of double mutant cycles it still exhibited significant coupling energies with the hot-spot residues from Cdc25B (1.3 – 2.2 kcal/mol). As we have previously shown that the C-terminal tail specifically contributes a factor of 10 to substrate recognition (44), removal of this remote region serves as an ideal control in the double mutant cycle experiments. Thus, as expected, assays of C-terminally truncated Cdc25B exhibit simple additivity and no significant coupling energy when assayed with the D206A or D210A mutant of Cdk2 (Table 2).

DISCUSSION

Computational protein-protein docking is a difficult problem, and its successful application to a real biological

problem is rare. The difficulty arises mostly because high accuracy is required to arrive at sufficiently correct molecular details to predict the outcome of experimentation by mutagenesis. As evidenced by recent CAPRI docking prediction contests, the winning entries identify less than 50% of the contact residues between the two proteins and have rmsds from the correct solution of >4 Å. Additionally, we and others have found that applying computationally expensive MD simulations to rigid docking solutions differing by less than 2 Å rmsd can result in different refined solutions (e.g., model 1 vs model 2). For the experimentalist, difficulties in protein docking are exacerbated because hot-spot residues whose mutation significantly affects protein–protein interactions make up only a small fraction of total interfacial residues (8). This is in agreement with our findings for the recognition of protein substrate by Cdc25B. Cdc25 and the Cdk-pTpY–CycA complex form a large protein interface, burying 3800 Å² of solvent accessible surface area, in comparison to an average protein interface of 1600 Å² (45). Of the 16 mutants of Cdc25B we have examined thus far, only three contribute more than 10-fold specifically to enhancing activity versus protein substrate, although 13 of them make contact with Cdk2 in our refined model. For example, Tyr382 interacts at a distance only slightly greater than that of hot-spot residue Tyr497 with Asp210 of Cdk2, yet the Y382A mutation has a relatively minor effect on activity with protein substrate (14% remaining activity) (6). Similarly, although in our model Gln396 in Cdc25B forms a hydrogen bond with Thr165 in Cdk2 and Glu534 in Cdc25B forms a salt bridge with Lys289 in CycA, mutation of either of these residues in Cdc25B does not significantly affect activity with the protein substrate (6). Thus, in accord with other protein–protein interactions, including binding of human growth hormone to its receptor (46) or binding of barnase to its inhibitor (41), we also find just a few hot-spot residues surrounded by a larger number of amino acids whose mutation does not significantly affect the binding specificity.

Our predicted docking orientation for binding of Cdc25 to the Cdk2–CycA complex is consistent with the C-terminal lobe of Cdk2 being a site for multiple protein–protein interactions, including the other Cdc25s (Cdc25A and Cdc25C), the kinase-associated phosphatase (KAP), and CksHs1. In fact, an analogy can be made between the hot-spot region on Cdk2 and the so-called common docking site of the MAP kinase pathway (47). For example, the general docking scheme seen in the crystal structure of KAP bound to Cdk2-pThr160 shows a striking similarity to our model of Cdc25B bound to the Cdk2-pTpY–CycA complex (48). Although sharing no overall sequence or fold homology with Cdc25, KAP is also a cysteine-containing phosphatase of the tyrosine phosphatase family. Like that of the Cdc25 interaction with Cdk2, the major site of interaction between KAP and Cdk2 lies in the C-terminal lobe and is far from the site of dephosphorylation. Although the detailed interactions at the remote site are different, a few of the same residues in Cdk2 appear to be involved in interacting with KAP as with Cdc25B, Asp206 in particular. However, for KAP, it is not known which residues contribute energetically to substrate recognition. This same region in the C-terminal lobe of Cdk2 is also known to interact with CksHs1 (49), a member of the Suc family of proteins involved in degradation of cell cycle proteins through the SCF ubiquitin ligase (50).

Specifically, Asp206 on Cdk2 is seen to interact with Tyr7 and His21 of CksHs1, although the effect of mutating these residues on binding of CksHs1 has not been measured. Earlier studies have demonstrated that the yeast homologue of CksHs1 (p13suc1) inhibits Cdc2 dephosphorylation on Tyr15 (51), an observation that seemed cryptic when the structure of CksHs1 bound to Cdk2 was first reported. Our model indicating an overlap of the Cdc25 and CksHs1 binding sites on Cdk2 is consistent with these results, as is the observed slowed growth rate and cell elongation upon overexpression of p13suc1 (52). However, it does raise the question of how Cdc25 can gain access to the Cdk–Cyc complexes inside the cell since the Suc proteins are known to bind to Cdks with at least nanomolar affinity. Given the multiple interactions that can exist at this docking site on Cdk2, it seems that a more detailed accounting of what complexes actually exist inside the cell is warranted if we are to fully understand cell cycle regulation.

The identity of the catalytic acid for the Cdc25 reaction remains an important unanswered question in our model. We have previously shown that neither Glu474 nor Glu478 of Cdc25 could serve as a catalytic acid (20), in good agreement with the details of our predicted active site region. Glu478, whose mutation to Gln had no effect on activity with protein substrate, faces away from the active site and makes a salt bridge with Lys394 (not shown). Glu474, whose mutation to Gln or Ala reduced activity with protein substrate by a factor of 200 without changing the pH–rate profile, is in tight hydrogen bonding contact with Arg36 of Cdk2 (Figure 5). In fact, its approach to the leaving group oxygen (O_γ) of pThr14 appears to be precluded by the π -cation packing of Phe475 of Cdc25 to Arg36 of Cdk2. From our model, it appears that Arg36 is best situated to donate a proton to the leaving group oxygen, in agreement with earlier data supporting substrate-assisted catalysis for the reaction of Cdc25B with the protein substrate (53, 54). However, the R36L mutant retains full activity and an unperturbed pH–rate profile (data not shown). Consistent with their lack of homology to other PTPs, perhaps the Cdc25s have developed a novel mechanism that does not involve a catalytic acid.

In closing, it should be cautioned that although we began our docking studies using two high-resolution structures, our docked orientation for the Cdk2–CycA–Cdc25B complex is only a working model and not in itself a high-resolution structure. Thus, we expect that many details will be inaccurate and that a true cocrystal structure will be useful in gaining further insight into these details. However, this docked orientation, with its broad interaction surface involving numerous binding interactions remote from the active sites of either Cdc25 or Cdk2, suggests that several potential small molecule binding pockets are available to achieve inhibition of dephosphorylation by blocking protein association. Thus, our results raise new possibilities for the screening or design of specific inhibitors of this protein–protein interaction that is associated with rapid cell growth and cancer.

SUPPORTING INFORMATION AVAILABLE

Data collection and refinement statistics for the active site C473S mutant of the catalytic domain of Cdc25B. This material is available free of charge via the Internet at <http://pubs.acs.org>.

REFERENCES

- Kristjánisdóttir, K., and Rudolph, J. (2004) Cdc25 phosphatases and cancer, *Chem. Biol.* 11, 1043–1051.
- Iliakis, G., Wang, Y., Guan, J., and Wang, H. (2003) DNA damage checkpoint control in cells exposed to ionizing radiation, *Oncogene* 22, 5834–5847.
- Fauman, E. B., Cogswell, J. P., Lovejoy, B., Rocque, W. J., Holmes, W., Montana, V. G., Pivnicka-Worms, H., Rink, M. J., and Saper, M. A. (1998) Crystal structure of the catalytic domain of the human cell cycle control phosphatase, Cdc25A, *Cell* 93, 617–625.
- Reynolds, R. A., Yem, A. W., Wolfe, C. L., Deibel, M. R. J., Chidester, C. G., and Watenpaugh, K. D. (1999) Crystal structure of the catalytic subunit of Cdc25B required for G2/M phase transition of the cell cycle, *J. Mol. Biol.* 293, 559–568.
- Rudolph, J., Epstein, D. M., Parker, L., and Eckstein, J. (2001) Specificity of natural and artificial substrates for human Cdc25A, *Anal. Biochem.* 289, 43–51.
- Sohn, J., Kristjánisdóttir, K., Safi, A., Parker, B., Kiburz, B., and Rudolph, J. (2004) Remote hotspots mediate protein substrate recognition for the Cdc25 phosphatase, *Proc. Natl. Acad. Sci. U.S.A.* 47, 16437–16441.
- Janin, J., Henrick, K., Moulton, J., Eyck, L. T., Sternberg, M. J. E., Vajda, S., Vakser, I., and Wodak, S. J. (2003) CAPRI: A Critical Assessment of PRedicted Interactions, *Proteins* 52, 2–9.
- Bogan, A. A., and Thorn, K. S. (1998) Anatomy of hot spots in protein interfaces, *J. Mol. Biol.* 280, 1–9.
- Jeffrey, P. D., Russo, A. A., Polyak, K., Gibbs, E., Hurwitz, J., Massagué, J., and Pavletich, N. P. (1995) Mechanism of CDK activation revealed by the structure of a CyclinA-CDK2 complex, *Nature* 376, 313–320.
- Wang, Y., Agarwal, P. K., Edelsbrunner, H., and Rudolph, J. (2005) Coarse and reliable geometric alignment for protein docking, *Pac. Symp. Biocomput.* 2005, 64–75.
- Agarwal, P. K., Edelsbrunner, H., Harer, J., and Wang, Y. (2004) Extreme elevation on a 2-manifold, *Proc. 20th Ann. Symp. Comput. Geom.*, 357–365.
- Choi, V., Agarwal, P. K., Edelsbrunner, H., and Rudolph, J. (2004) Local search heuristic for rigid protein docking, *4th Workshop on Algorithms in Bioinformatics (WABI), Lecture Notes in Computer Science* 3240, 218–229.
- Davis, I. W., Murray, L. W., Richardson, J. S., and Richardson, D. C. (2004) MOLPROBITY: Structure validation and all-atom contact analysis for nucleic acids and their complexes, *Nucleic Acids Res.* 32, W615–W619.
- Jorgensen, W. L., Chandrasekhar, J., Madura, J. D., Impey, R. W., and Klein, M. L. (1983) Comparison of simple potential functions for simulating liquid water, *J. Chem. Phys.* 79, 926–935.
- Darden, T., York, D., and Pedersen, L. (1993) Particle mesh Ewald: An N·log(N) method for Ewald sums in large systems, *J. Chem. Phys.* 98, 10089–10092.
- Anderson, H. C. (1983) Rattle: A velocity version of the SHAKE algorithm for molecular dynamics calculations, *J. Comput. Phys.* 52, 24–34.
- MacKerrell, A. D., Jr., et al. (1998) All-Atom Empirical Potential for Molecular Modeling and Dynamics Studies of Proteins, *J. Phys. Chem. B* 102, 3586–3616.
- Feng, M. H., Philippopoulos, M., MacKerrell, A. D., Jr., and Lim, C. (1996) Structural characterization of the phosphotyrosine binding region of a high affinity SH2 domain-phosphopeptide complex by molecular dynamics simulation and chemical shift calculations, *J. Am. Chem. Soc.* 118, 11265–11277.
- Kalé, L., Skeel, R., Bhandarkar, M., Brunner, R., Gursoy, A., Krawetz, N., Phillips, J., Shinozaki, A., Varadarajan, K., and Schulten, K. (1999) NAMD2: Greater scalability for parallel molecular dynamics, *J. Comput. Phys.* 151, 283–312.
- Chen, W., Wilborn, M., and Rudolph, J. (2000) Dual-specific Cdc25B phosphatase: In search of the catalytic acid, *Biochemistry* 39, 10781–10789.
- Buhrman, G., Parker, B., Sohn, J., Rudolph, J., and Mattos, C. (2005) Structural mechanism of oxidative regulation of the phosphatase Cdc25B vis an intramolecular disulfide bond, *Biochemistry* 44, 5307–5316.
- Brunger, A. T., Adams, P. D., Clore, G. M., DeLano, W. L., Gros, P., Grosse-Kunstleve, R. W., Jiang, J. S., Kuszewski, J., Nilges, M., Pannu, N. S., Read, R. J., Rice, L. M., Simonson, T., and Warren, G. L. (1998) Crystallography & NMR system: A new software suite for macromolecular structure determination, *Acta Crystallogr. D* 54, 905–921.
- Brunger, A. T. (1997) Free R value: Cross-validation in crystallography, *Methods Enzymol.* 277, 366–396.
- Jones, T. A., Zhou, J. Y., Cowan, S. W., and Kjeldgaard, M. (1991) Improved methods for building protein models in electron density maps and the location of errors in these models, *Acta Crystallogr. A* 47, 110–119.
- Cleland, W. W. (1979) Statistical analysis of enzyme kinetic data, *Methods Enzymol.* 63, 103–138.
- Pons, J., Rajpal, A., and Kirsch, H. F. (1999) Energetic analysis of an antigen/antibody interface: Alanine scanning mutagenesis and double mutant cycles on the HyHEL-10/lysozyme interaction, *Protein Sci.* 8, 958–968.
- Theesfeld, C. L., Zyla, T. R., Bardes, E. S. G., and Lew, D. J. (2003) A monitor for bud emergence in the yeast morphogenesis checkpoint, *Mol. Biol. Cell* 14, 3280–3291.
- Chen, R., Mintseris, J., Janin, J., and Weng, Z. (2003) A protein–protein docking benchmark, *Proteins* 51, 88–91.
- Xu, X., and Burke, S. P. (1996) Roles of active site residues and the NH2-terminal domain in the catalysis and substrate binding of human Cdc25, *J. Biol. Chem.* 271, 5118–5124.
- Borgne, A., and Meijer, L. (1996) Sequential dephosphorylation of p34cdc2 on Thr-14 and Tyr-15 at the prophase/metaphase transition, *J. Biol. Chem.* 271, 27847–27854.
- Scapin, G., Patel, S., Patel, V., Kennedy, B., and Asante-Appiah, E. (2001) The structure of apo protein-tyrosine phosphatase 1B C215S mutant: More than just an S → O change, *Protein Sci.* 10, 1596–1605.
- Gautier, J., Solomon, M. J., Booher, R. N., Bazan, J. F., and Kirschner, M. W. (1991) Cdc25 Is a specific tyrosine phosphatase that directly activates p34cdc2, *Cell* 67, 197–211.
- Lee, M. S., Ogg, S., Xu, M., Parker, L. L., Donoghue, D. J., Maller, J. L., and Pivnicka-Worms, H. (1992) cdc25+ encodes a protein phosphatase that dephosphorylates p34cdc2, *Mol. Biol. Cell* 3, 73–84.
- Clackson, T., and Wells, J. A. (1995) A hot spot of binding energy in a hormone-receptor interface, *Science* 267, 383–6.
- Goldman, E. R., Dall'Acqua, W., Braden, B. C., and Mariuzza, R. A. (1997) Analysis of binding interaction in an idiotope-antidiotope protein–protein complex by double mutant cycles, *Biochemistry* 36, 49–56.
- Dall'Acqua, W., Goldman, E. R., Lin, W., Teng, C., Tsuchiya, D., Li, H., Ysern, X., Braden, B. C., Li, Y., Smith-Gill, S. J., and Mariuzza, R. A. (1998) A mutational analysis of binding interactions in an antigen–antibody protein–protein complex, *Biochemistry* 37, 7981–7991.
- Carter, P. J., Winter, G., Wilkinson, A. J., and Fersht, A. R. (1984) The use of double mutants to detect structural changes in the active site of the tyrosyl-tRNA synthetase (*Bacillus stearothermophilus*), *Cell* 38, 835–840.
- Mildvan, A. S., Weber, D. J., and Kuliopulos, A. (1992) Quantitative interpretation of double mutations of enzymes, *Arch. Biochem. Biophys.* 294, 327–340.
- Wells, J. A. (1990) Additivity of mutational effects in proteins, *Biochemistry* 29, 8509–8517.
- Horovitz, A. (1996) Double-mutant cycles: A powerful tool for analyzing protein structure and function, *Folding Des.* 1, R121–R126.
- Schreiber, S., and Fersht, A. R. (1995) Energetics of protein–protein interactions: Analysis of the barnase-barstar interface by single mutations and double mutant cycles, *J. Mol. Biol.* 248, 478–486.
- Hidalgo, P., and MacKinnon, R. (1995) Revealing the architecture of a K⁺ channel pore through mutant cycles with a peptide inhibitor, *Science* 268, 307–310.
- Reichmann, D., Rahat, O., Albeck, S., Meged, R., Dym, O., and Schreiber, G. (2005) The modular architecture of protein–protein binding interfaces, *Proc. Natl. Acad. Sci. U.S.A.* 102, 57–62.
- Wilborn, M., Free, S., Ban, A., and Rudolph, J. (2001) The C-terminal tail of the dual-specificity Cdc25B phosphatase mediates modular substrate recognition, *Biochemistry* 40, 14200–14206.
- Lo Conte, L., Chothia, C., and Janin, J. (1999) The atomic structure of protein–protein recognition sites, *J. Mol. Biol.* 285, 2177–2198.
- Wells, J. A. (1996) Binding in the growth hormone receptor complex, *Proc. Natl. Acad. Sci. U.S.A.* 93, 1–6.

47. Tanoue, T., and Nishida, E. (2003) Molecular recognitions in the MAP kinase cascades, *Cell Signalling* 15, 455–462.
48. Song, H., Hanlon, N., Brown, N. R., Noble, M. E. M., Johnson, L. N., and Barford, D. (2001) Phosphoprotein–protein interactions revealed by the crystal structure of kinase-associated phosphatase in complex with phospho-Cdk2, *Mol. Cell* 7, 615–626.
49. Bourne, Y., Watson, M. H., Hickey, M. J., Holmes, W., Rocque, W., Reed, S. I., and Tainer, J. A. (1996) Crystal structure and mutational analysis of the human cdk2 kinase complex with cell cycle-regulatory protein CksHs1, *Cell* 84, 863–874.
50. Cardozo, T., and Pagano, M. (2004) The SCF ubiquitin ligase: Insights into a molecular machine, *Nat. Rev. Mol. Cell Biol.* 5, 739–751.
51. Dunphy, W. G., and Newport, J. W. (1989) Fission yeast p13 blocks mitotic activation and tyrosine dephosphorylation of the *Xenopus* cdc2 protein kinase, *Cell* 58, 181–191.
52. Hayles, J., Aves, S., and Nurse, P. (1986) *suc1* is an essential gene involved in both the cell cycle and growth in fission yeast, *EMBO J.* 5, 3373–3379.
53. Rudolph, J. (2002) Catalytic mechanism of Cdc25, *Biochemistry* 41, 14613–14623.
54. Rudolph, J. (2005) Reactivity of Cdc25 phosphatase at low pH and with thiophosphorylated protein substrate, *Bioorg. Chem.* 33, 264–273.

BI0516879